Revisiting Generalized Two Higgs Doublet Model in the Light of Muon Anomaly and Lepton Flavor Violating Decays at HL-LHC

Nivedita Ghosh
RECAPP, HRI, A CI of Homi Bhabha National Institute, India

Presented in KIAS

September 22, 2022

Outline

Based on the work:
Revisiting Generalized Two Higgs Doublet Model in the Light of Muon Anomaly and Lepton Flavor Violating Decays at HL-LHC (Phys.Rev.D 103 (2021) 5, 05500), **NG**, Jayita Lahiri

Motivation

- Anomalous magnetic moment of muon is a crucial observation which calls for new physics.

[1] 1501.06858, MUON G-2 Collaboration
[2] J. Phys. Conf. Ser. 295 (2011) 012032, EDM collaboration
[3] Phys. Rept. 731 (2018) 1–82, Lindler et al.

Motivation

- Anomalous magnetic moment of muon is a crucial observation which calls for new physics.
- Ongoing E989 experiment at Fermilab [1] and future E34 experiment at J-PARC [2] are expected to shed new light on this tension between the theory and data.

[1] 1501.06858, MUON G-2 Collaboration
[2] J. Phys. Conf. Ser. 295 (2011) 012032, EDM collaboration
[3] Phys. Rept. 731 (2018) 1–82, Lindler et al.

Motivation

- Anomalous magnetic moment of muon is a crucial observation which calls for new physics.
- Ongoing E989 experiment at Fermilab [1] and future E34 experiment at J-PARC [2] are expected to shed new light on this tension between the theory and data.
- Lepton Flavor violation (LFV) has not yet been observed in the charged lepton sector.

[1] 1501.06858, MUON G-2 Collaboration
[2] J. Phys. Conf. Ser. 295 (2011) 012032, EDM collaboration
[3] Phys. Rept. 731 (2018) 1–82, Lindler et al.

Motivation

- Anomalous magnetic moment of muon is a crucial observation which calls for new physics.
- Ongoing E989 experiment at Fermilab [1] and future E34 experiment at J-PARC [2] are expected to shed new light on this tension between the theory and data.
- Lepton Flavor violation (LFV) has not yet been observed in the charged lepton sector.
- Various low energy experiments have put strong bounds on branching ratios of flavor changing neutral current(FCNC) decays and correspondingly on the associated couplings.

[1] 1501.06858, MUON G-2 Collaboration
[2] J. Phys. Conf. Ser. 295 (2011) 012032, EDM collaboration
[3] Phys. Rept. 731 (2018) 1–82, Lindler et al.

Motivation

- Anomalous magnetic moment of muon is a crucial observation which calls for new physics.
- Ongoing E989 experiment at Fermilab [1] and future E34 experiment at J-PARC [2] are expected to shed new light on this tension between the theory and data.
- Lepton Flavor violation (LFV) has not yet been observed in the charged lepton sector.
- Various low energy experiments have put strong bounds on branching ratios of flavor changing neutral current(FCNC) decays and correspondingly on the associated couplings.
- Experimental observation of muon anomaly and non-observation of lepton flavor violation will definitely create a tension in terms of the allowed parameter space for various candidate models [3] which satisfy these two results individually.

[1] 1501.06858, MUON G-2 Collaboration
[2] J. Phys. Conf. Ser. 295 (2011) 012032, EDM collaboration
[3] Phys. Rept. 731 (2018) 1–82, Lindler et al.

Motivation

- Anomalous magnetic moment of muon is a crucial observation which calls for new physics.
- Ongoing E989 experiment at Fermilab [1] and future E34 experiment at J-PARC [2] are expected to shed new light on this tension between the theory and data.
- Lepton Flavor violation (LFV) has not yet been observed in the charged lepton sector.
- Various low energy experiments have put strong bounds on branching ratios of flavor changing neutral current(FCNC) decays and correspondingly on the associated couplings.
- Experimental observation of muon anomaly and non-observation of lepton flavor violation will definitely create a tension in terms of the allowed parameter space for various candidate models [3] which satisfy these two results individually.
- In this work our goal is to satisfy both of these observations simultaneously and also, to look for signatures of lepton flavor violation in the collider experiments.

[1] 1501.06858, MUON G-2 Collaboration

[2] J. Phys. Conf. Ser. 295 (2011) 012032, EDM collaboration

[3] Phys. Rept. 731 (2018) 1–82, Lindler et al.

Two scalar doublets Φ_1 and Φ_2 with hyper charge $Y = 1$ [4] are present in this model [5].

[4] $Q = T_3 + \frac{Y}{2}$.
[5] JHEP 05 (2017) 055, Primulendo et al

Two scalar doublets Φ_1 and Φ_2 with hyper charge $Y = 1$ [4] are present in this model [5]. The most general scalar potential can be written as:

$$\begin{aligned}\mathcal{V}_{2HDM} = & M_{11}^2(\Phi_1^\dagger\Phi_1) + M_{22}^2(\Phi_2^\dagger\Phi_2) - [M_{12}^2(\Phi_1^\dagger\Phi_2) + \text{h.c.}] \\ & + \frac{1}{2}\lambda_1(\Phi_1^\dagger\Phi_1)^2 + \frac{1}{2}\lambda_2(\Phi_2^\dagger\Phi_2)^2 + \lambda_3(\Phi_1^\dagger\Phi_1)(\Phi_2^\dagger\Phi_2) + \lambda_4(\Phi_1^\dagger\Phi_2)(\Phi_2^\dagger\Phi_1) \\ & + \{\frac{1}{2}\lambda_5(\Phi_1^\dagger\Phi_2)^2 + [\lambda_6(\Phi_1^\dagger\Phi_1) + \lambda_7(\Phi_2^\dagger\Phi_2)](\Phi_1^\dagger\Phi_2) + \text{h.c.}\}.\end{aligned} \tag{1}$$

[4] $Q = T_3 + \frac{Y}{2}$.
[5] JHEP 05 (2017) 055, Primulendo et al

Two scalar doublets Φ_1 and Φ_2 with hyper charge $Y = 1$ [4] are present in this model [5].
The most general scalar potential can be written as:

$$\begin{aligned}\mathcal{V}_{2HDM} &= M_{11}^2(\Phi_1^\dagger\Phi_1) + M_{22}^2(\Phi_2^\dagger\Phi_2) - [M_{12}^2(\Phi_1^\dagger\Phi_2) + \text{h.c.}] \\ &+ \frac{1}{2}\lambda_1(\Phi_1^\dagger\Phi_1)^2 + \frac{1}{2}\lambda_2(\Phi_2^\dagger\Phi_2)^2 + \lambda_3(\Phi_1^\dagger\Phi_1)(\Phi_2^\dagger\Phi_2) + \lambda_4(\Phi_1^\dagger\Phi_2)(\Phi_2^\dagger\Phi_1) \\ &+ \{\frac{1}{2}\lambda_5(\Phi_1^\dagger\Phi_2)^2 + [\lambda_6(\Phi_1^\dagger\Phi_1) + \lambda_7(\Phi_2^\dagger\Phi_2)](\Phi_1^\dagger\Phi_2) + \text{h.c.}\}.\end{aligned} \tag{1}$$

The two scalar doublets of the model can be expanded as

$$\Phi_1 = \begin{pmatrix} \phi_1^+ \\ \frac{1}{\sqrt{2}}\left(Re[\Phi_1^0] + iIm[\Phi_1^0]\right) \end{pmatrix}, \qquad \Phi_2 = \begin{pmatrix} \phi_2^+ \\ \frac{1}{\sqrt{2}}\left(Re[\Phi_2^0] + iIm[\Phi_2^0]\right) \end{pmatrix}, \tag{2}$$

[4] $Q = T_3 + \frac{Y}{2}$.
[5] JHEP 05 (2017) 055, Primulendo et al

Two scalar doublets Φ_1 and Φ_2 with hyper charge $Y = 1$ [4] are present in this model [5]. The most general scalar potential can be written as:

$$\begin{aligned}\mathcal{V}_{2HDM} &= M_{11}^2(\Phi_1^\dagger\Phi_1) + M_{22}^2(\Phi_2^\dagger\Phi_2) - [M_{12}^2(\Phi_1^\dagger\Phi_2) + \text{h.c.}] \\ &+ \frac{1}{2}\lambda_1(\Phi_1^\dagger\Phi_1)^2 + \frac{1}{2}\lambda_2(\Phi_2^\dagger\Phi_2)^2 + \lambda_3(\Phi_1^\dagger\Phi_1)(\Phi_2^\dagger\Phi_2) + \lambda_4(\Phi_1^\dagger\Phi_2)(\Phi_2^\dagger\Phi_1) \\ &+ \{\frac{1}{2}\lambda_5(\Phi_1^\dagger\Phi_2)^2 + [\lambda_6(\Phi_1^\dagger\Phi_1) + \lambda_7(\Phi_2^\dagger\Phi_2)](\Phi_1^\dagger\Phi_2) + \text{h.c.}\}.\end{aligned} \tag{1}$$

The two scalar doublets of the model can be expanded as

$$\Phi_1 = \begin{pmatrix} \phi_1^+ \\ \frac{1}{\sqrt{2}}\left(Re[\Phi_1^0] + iIm[\Phi_1^0]\right) \end{pmatrix}, \qquad \Phi_2 = \begin{pmatrix} \phi_2^+ \\ \frac{1}{\sqrt{2}}\left(Re[\Phi_2^0] + iIm[\Phi_2^0]\right) \end{pmatrix}, \tag{2}$$

$$\langle\Phi_1\rangle = \frac{1}{\sqrt{2}}\begin{pmatrix} 0 \\ v_1 \end{pmatrix}, \qquad \langle\Phi_2\rangle = \frac{1}{\sqrt{2}}\begin{pmatrix} 0 \\ v_2 \end{pmatrix}. \tag{3}$$

A key parameter of the model is $\tan\beta = \frac{v_2}{v_1}$.

---

[4] $Q = T_3 + \frac{Y}{2}$.

[5] JHEP 05 (2017) 055, Primulendo et al

Model

$$\begin{pmatrix} \phi_1^{\pm} \\ \phi_2^{\pm} \end{pmatrix} = \begin{pmatrix} \cos\beta & \sin\beta \\ -\sin\beta & \cos\beta \end{pmatrix} \begin{pmatrix} H^{\pm} \\ G^{\pm} \end{pmatrix}, \tag{4}$$

$$\begin{pmatrix} \sqrt{2} Im[\Phi_1^0] \\ \sqrt{2} Im[\Phi_2^0] \end{pmatrix} = \begin{pmatrix} \cos\beta & \sin\beta \\ -\sin\beta & \cos\beta \end{pmatrix} \begin{pmatrix} A \\ G^0 \end{pmatrix}, \tag{5}$$

Model

$$\begin{pmatrix} \phi_1^{\pm} \\ \phi_2^{\pm} \end{pmatrix} = \begin{pmatrix} \cos\beta & \sin\beta \\ -\sin\beta & \cos\beta \end{pmatrix} \begin{pmatrix} H^{\pm} \\ G^{\pm} \end{pmatrix}, \tag{4}$$

$$\begin{pmatrix} \sqrt{2} Im[\Phi_1^0] \\ \sqrt{2} Im[\Phi_2^0] \end{pmatrix} = \begin{pmatrix} \cos\beta & \sin\beta \\ -\sin\beta & \cos\beta \end{pmatrix} \begin{pmatrix} A \\ G^0 \end{pmatrix}, \tag{5}$$

$$\begin{pmatrix} \sqrt{2} Re[\Phi_1^0] - v_1 \\ \sqrt{2} Re[\Phi_2^0] - v_2 \end{pmatrix} = \begin{pmatrix} \cos\alpha & \sin\alpha \\ -\sin\alpha & \cos\alpha \end{pmatrix} \begin{pmatrix} h \\ H \end{pmatrix}, \tag{6}$$

Model

$$\begin{pmatrix} \phi_1^{\pm} \\ \phi_2^{\pm} \end{pmatrix} = \begin{pmatrix} \cos\beta & \sin\beta \\ -\sin\beta & \cos\beta \end{pmatrix} \begin{pmatrix} H^{\pm} \\ G^{\pm} \end{pmatrix}, \tag{4}$$

$$\begin{pmatrix} \sqrt{2}Im[\Phi_1^0] \\ \sqrt{2}Im[\Phi_2^0] \end{pmatrix} = \begin{pmatrix} \cos\beta & \sin\beta \\ -\sin\beta & \cos\beta \end{pmatrix} \begin{pmatrix} A \\ G^0 \end{pmatrix}, \tag{5}$$

$$\begin{pmatrix} \sqrt{2}Re[\Phi_1^0] - v_1 \\ \sqrt{2}Re[\Phi_2^0] - v_2 \end{pmatrix} = \begin{pmatrix} \cos\alpha & \sin\alpha \\ -\sin\alpha & \cos\alpha \end{pmatrix} \begin{pmatrix} h \\ H \end{pmatrix}, \tag{6}$$

Where either h or H is assumed to behave like the Higgs of Standard Model with mass 125 GeV.

Model

In general, a Z_2 symmetry is imposed to avoid tree-level FCNC.

Model	u_R^i	d_R^i	e_R^i
Type I	Φ_2	Φ_2	Φ_2
Type II	Φ_2	Φ_1	Φ_1
Lepton-specific	Φ_2	Φ_2	Φ_1
Flipped	Φ_2	Φ_1	Φ_2

Model

Unlike these aforementioned types of 2HDM, in the generalized 2HDM, no Z_2 symmetry is imposed on the Lagrangian $\rightarrow$ **tree $-$ level FCNC**.

$$-\mathcal{L}_{Yukawa} = \bar{Q}_L(Y_1^d\Phi_1+Y_2^d\Phi_2)d_R+\bar{Q}_L(Y_1^u\tilde{\Phi}_1+Y_2^u\tilde{\Phi}_2)u_R+\bar{L}_L(Y_1^\ell\Phi_1+Y_2^\ell\Phi_2)e_R+h.c. \tag{7}$$

Model

Unlike these aforementioned types of 2HDM, in the generalized 2HDM, no Z_2 symmetry is imposed on the Lagrangian $\rightarrow$ **tree − level FCNC**.

$$-\mathcal{L}_{Yukawa} = \bar{Q}_L(Y_1^d\Phi_1 + Y_2^d\Phi_2)d_R + \bar{Q}_L(Y_1^u\tilde{\Phi}_1 + Y_2^u\tilde{\Phi}_2)u_R + \bar{L}_L(Y_1^\ell\Phi_1 + Y_2^\ell\Phi_2)e_R + h.c. \tag{7}$$

Expanding in terms of the VEVs and physical fields, we can get the fermion mass matrix

Model

Unlike these aforementioned types of 2HDM, in the generalized 2HDM, no Z_2 symmetry is imposed on the Lagrangian $\rightarrow$ **tree $-$ level FCNC**.

$$-\mathcal{L}_{Yukawa} = \bar{Q}_L(Y_1^d\Phi_1 + Y_2^d\Phi_2)d_R + \bar{Q}_L(Y_1^u\tilde{\Phi}_1 + Y_2^u\tilde{\Phi}_2)u_R + \bar{L}_L(Y_1^\ell\Phi_1 + Y_2^\ell\Phi_2)e_R + h.c. \tag{7}$$

Expanding in terms of the VEVs and physical fields, we can get the fermion mass matrix

$$\bar{f}_L\mathbf{M}^f f_R = \bar{f}_L(\frac{v_1 Y_1^f}{\sqrt{2}} + \frac{v_2 Y_2^f}{\sqrt{2}})f_R + h.c. \tag{8}$$

Model

Diagonalize Y_2^u , Y_2^d and Y_1^ℓ matrices where others remain non-diagonal leading to tree- level FCNC in the Yukawa sector. We consider the Yukawa Lagrangian as a perturbation of Type X model in terms of FCNC couplings [6].

$$\begin{aligned}
-\mathcal{L}^{\phi}_{Yukawa} &= \bar{u}_L \left[\left(\frac{c_\alpha \mathbf{m}^u}{v s_\beta} - \frac{c_{\beta-\alpha}\Sigma^u}{\sqrt{2}s_\beta} \right) h + \left(\frac{s_\alpha \mathbf{m}^u}{s_\beta v} + \frac{s_{\beta-\alpha}\Sigma^u}{\sqrt{2}s_\beta} \right) H \right] u_R \\
&+ \bar{d}_L \left[\left(\frac{c_\alpha \mathbf{m}^d}{v s_\beta} - \frac{c_{\beta-\alpha}\Sigma^d}{\sqrt{2}s_\beta} \right) h + \left(\frac{s_\alpha \mathbf{m}^d}{s_\beta v} + \frac{s_{\beta-\alpha}\Sigma^d}{\sqrt{2}s_\beta} \right) H \right] d_R \\
&+ \bar{e}_L \left[\left(-\frac{s_\alpha \mathbf{m}^\ell}{v c_\beta} + \frac{c_{\beta-\alpha}\Sigma^\ell}{\sqrt{2}c_\beta} \right) h + \left(\frac{c_\alpha \mathbf{m}^\ell}{c_\beta v} - \frac{s_{\beta-\alpha}\Sigma^\ell}{\sqrt{2}c_\beta} \right) H \right] e_R \\
&- i \left[\bar{u}_L \left(\frac{\mathbf{m}^u}{t_\beta v} - \frac{\Sigma^u}{\sqrt{2}s_\beta} \right) u_R + \bar{d}_L \left(-\frac{\mathbf{m}^d}{t_\beta v} + \frac{\Sigma^d}{\sqrt{2}s_\beta} \right) d_R \right] A \\
&- i \left[\bar{e}_L \left(\frac{t_\beta \mathbf{m}^\ell}{v} - \frac{\Sigma^\ell}{\sqrt{2}c_\beta} \right) e_R \right] A + h.c. \qquad (9)
\end{aligned}$$

[6] PhysRevLett.116.081801, Crivellin et al

Model

Here $\mathbf{m}^f = U_L^f \mathbf{M}^f U_R^f$ is the diagonal mass matrices of the fermions and U_L^f and U_R^f are the unitary matrices required to diagonalize $\mathbf{M}^f$, $\Sigma^u = U_L^u Y_1^u U_R^{\dagger u}$, $\Sigma^d = U_L^d Y_1^d U_R^{\dagger d}$ and $\Sigma^\ell = U_L^\ell Y_2^u U_R^{\dagger l}$.

[7] Phys. Rev. D35 (1987) 3484, Cheng et al

Model

Here $\mathbf{m}^f = U_L^f \mathbf{M}^f U_R^f$ is the diagonal mass matrices of the fermions and U_L^f and U_R^f are the unitary matrices required to diagonalize $\mathbf{M}^f$, $\Sigma^u = U_L^u Y_1^u U_R^{\dagger u}$, $\Sigma^d = U_L^d Y_1^d U_R^{\dagger d}$ and $\Sigma^\ell = U_L^\ell Y_2^u U_R^{\dagger l}$.
Following the convention of [7]

$$\Sigma_{ij}^f = \sqrt{m_i^f m_j^f}\chi_{ij}^f / v \tag{10}$$

Yukawa couplings of the charged Higgs boson are similar to those of the CP-odd scalar and can be written as

$$\begin{aligned} \mathcal{L}_Y^{H^\pm} = & \frac{\sqrt{2}}{v}\bar{u}_i \left(m_i^u (\xi^{u*})_{ki} V_{kj} P_L + V_{ik} (\xi^d)_{kj} m_j^d P_R \right) d_j H^+ \\ & + \frac{\sqrt{2}}{v} \bar{\nu}_i (\xi^\ell)_{ij} m_j^\ell P_R \ell_j H^+ + h.c. \end{aligned} \tag{11}$$

[7] Phys. Rev. D35 (1987) 3484, Cheng et al

Model

$$\xi^u = \frac{1}{t_\beta}\delta_{ij} - \frac{1}{\sqrt{2}s_\beta}\sqrt{\frac{m_i^u}{m_j^u}}\chi_{ij}^u, \tag{12}$$

$$\xi^d = -\frac{1}{t_\beta}\delta_{ij} + \frac{1}{\sqrt{2}s_\beta}\sqrt{\frac{m_i^d}{m_j^d}}\chi_{ij}^d, \tag{13}$$

$$\xi^\ell = t_\beta\delta_{ij} - \frac{1}{\sqrt{2}c_\beta}\sqrt{\frac{m_i^\ell}{m_j^\ell}}\chi_{ij}^\ell \tag{14}$$

$$a_{\mu}^{SM} = 116591810(43) \times 10^{-11} \tag{15}$$

Recently, the “MUON G-2” collaboration at Fermilab has published their result.

$$a_{\mu}^{exp-FNAL} = 116592040(54) \times 10^{-11} \tag{16}$$

The combined new world average(combination of recent FNAL and older BNL(2006) data) is published as

$$a_{\mu}^{exp-comb} = 116592061(41) \times 10^{-11} \tag{17}$$

The difference between the experimental observation and the SM prediction, defined as Δa_{μ}, amounts to a 4.2σ discrepancy, which urges us to look beyond the SM.

$$\Delta a_{\mu} = a_{\mu}^{exp-comb} - a_{\mu}^{SM} = 251(59) \times 10^{-11} \tag{18}$$

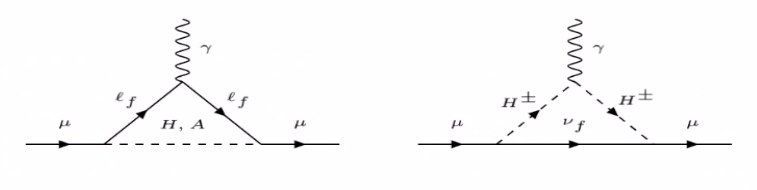
γ
ℓ_f
ℓ_f
H, A
μ
μ
γ
$H^{\pm}$
$H^{\pm}$
ν_f
μ
μ

Muon Anomaly

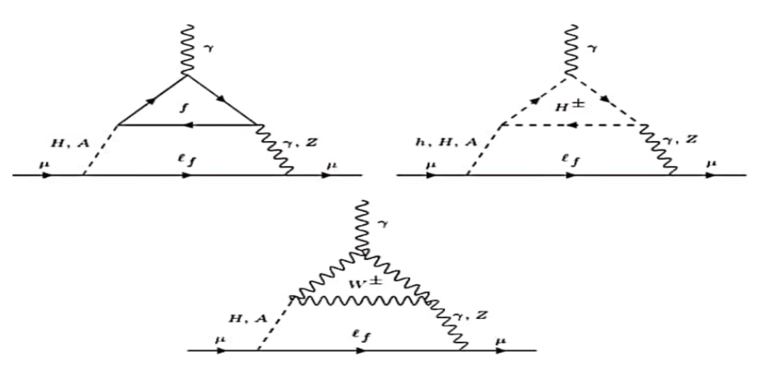

Muon Anomaly

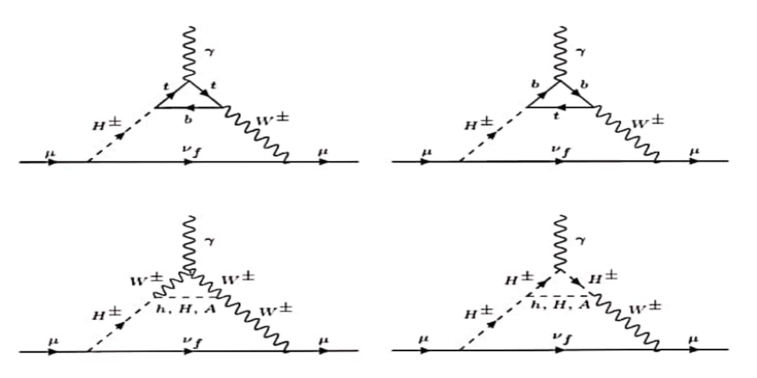

Muon Anomaly

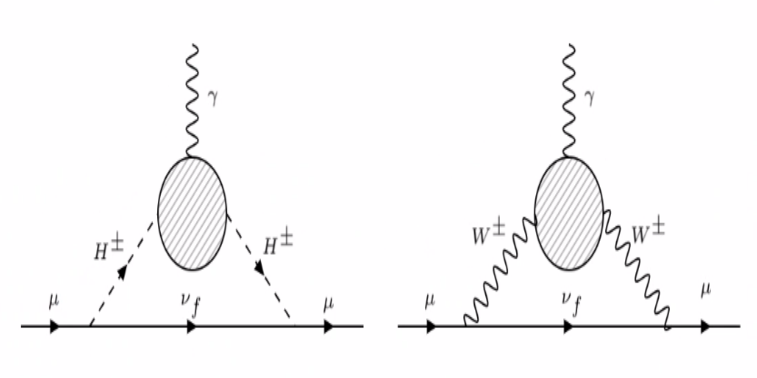

Muon Anomaly

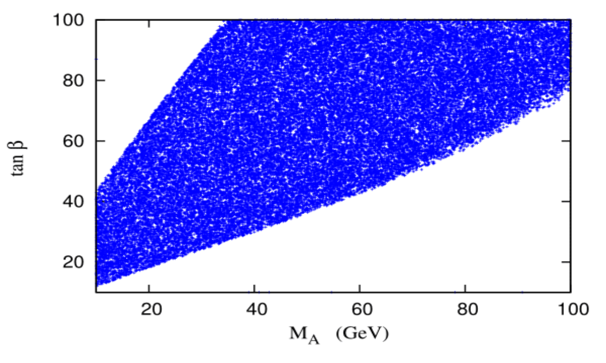

Figure: *The allowed region in $m_A - \tan\beta$ plane from $g_\mu - 2$ data at 3σ. The flavor changing couplings are taken to be $y_{\mu e} = 10^{-7}$, $y_{\tau e} = 5 \times 10^{-5}$, $y_{\mu\tau} = 5 \times 10^{-5}$. The non-standard neutral CP-even Higgs mass is 120 GeV and charged Higgs mass is 150 GeV.*

Muon Anomaly

One can check that a low mass pseudoscalar with an enhanced coupling to the C leptons will give significant contribution to muon anomaly.

Muon Anomaly

One can check that a low mass pseudoscalar with an enhanced coupling to the C leptons will give significant contribution to muon anomaly. In our model the coupling of pseudoscalar with a pair of V leptons is proportional to *tan*β. Therefore, *low m_A and large tanβ* region is favored in the light of muon anomaly data.

Low Energy Experiments

$BR(\mu \to e\gamma) < 4.2 \times 10^{-13}$ [8], $BR(\tau \to e\gamma) < 3.3 \times 10^{-8}$ and $BR(\tau \to \mu\gamma) < 4.4 \times 10^{-8}$

[8] MEG collaboration, EPJC 76 (2016) 434

Low Energy Experiments

$BR(\mu \to e\gamma) < 4.2 \times 10^{-13}$ [8], $BR(\tau \to e\gamma) < 3.3 \times 10^{-8}$ and $BR(\tau \to \mu\gamma) < 4.4 \times 10^{-8}$

$$CR(\mu \; Ti \to e \; Ti) \simeq \frac{1}{200} BR(\mu \to e\gamma) \tag{19}$$

$$BR(\mu \to 3e) \simeq \frac{1}{160} BR(\mu \to e\gamma) \tag{20}$$

[8] MEG collaboration, EPJC 76 (2016) 434

Low Energy Experiments

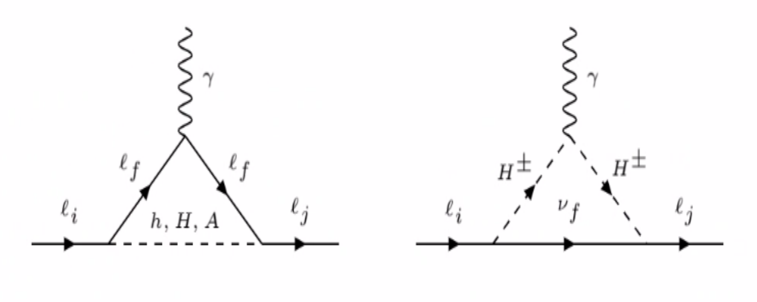

Low Energy Experiments

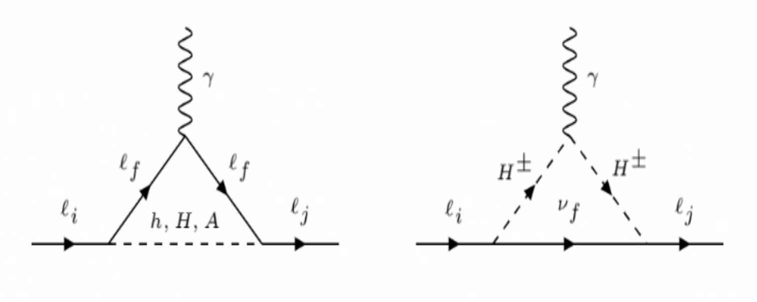

We have found that the two loop contribution to $\tau \to e\gamma$ and $\tau \to \mu\gamma$ amplitudes add up to mere $\sim 2\%$ of their one-loop counterpart. On the contrary, in case of $\mu \to e\gamma$, the addition of two loop contribution induces 3 times enhancement to the one-loop amplitude.

Low Energy Experiments

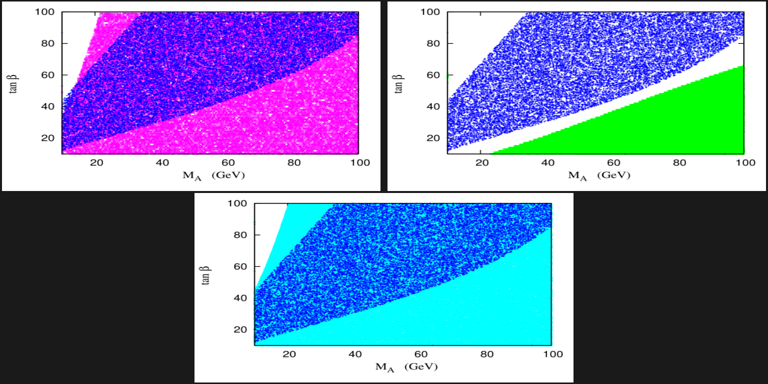

Figure: *The magenta, green and cyan regions are the allowed range for $\mu \to e\gamma$, $\tau \to e\gamma$ and $\tau \to \mu\gamma$ respectively.* $y_{\mu e} = 10^{-7}$, $y_{\tau e} = 10^{-4}$, $y_{\mu\tau} = 5 \times 10^{-5}$.

Low Energy Experiments

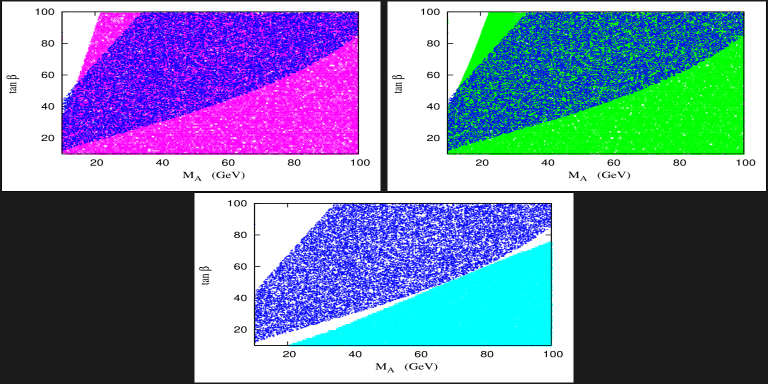

Figure: *The magenta, green and cyan regions are the allowed range for $\mu \to e\gamma$, $\tau \to e\gamma$ and $\tau \to \mu\gamma$ respectively.* $y_{\mu e} = 10^{-7}$, $y_{\tau e} = 5 \times 10^{-5}$, $y_{\mu\tau} = 10^{-4}$.

Low Energy Experiments

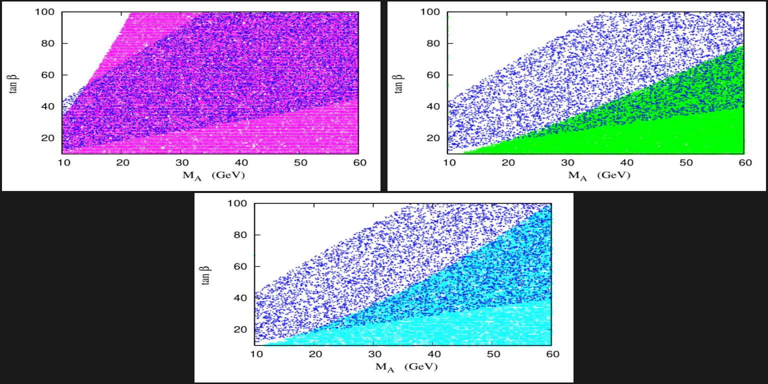

Figure: *The magenta, green and cyan regions are the allowed range for* $\mu \to e\gamma$, $\tau \to e\gamma$ *and* $\tau \to \mu\gamma$ *respectively.* $y_{\mu e} = 10^{-7}$, $y_{\tau e} = 5 \times 10^{-5}$, $y_{\mu\tau} = 5 \times 10^{-5}$.

Theoretical constraints

Vacuum stability requires

$$\lambda_1 > 0, \quad \lambda_2 > 0, \quad \lambda_3 > -\sqrt{\lambda_1 \lambda_2}, \quad \lambda_3 + \lambda_4 - |\lambda_5| > \sqrt{\lambda_1 \lambda_2} \tag{21}$$

Theoretical constraints

Vacuum stability requires

$$\lambda_1 > 0, \quad \lambda_2 > 0, \quad \lambda_3 > -\sqrt{\lambda_1\lambda_2}, \quad \lambda_3 + \lambda_4 - |\lambda_5| > \sqrt{\lambda_1\lambda_2} \tag{21}$$

$$m_A^2 = \frac{m_{12}^2}{s_\beta c_\beta} - \frac{1}{2}v^2(2\lambda_5 + \frac{\lambda_6}{t_\beta} + \lambda_7 t_\beta) \tag{22}$$

$$m_{H^\pm}^2 = m_A^2 + \frac{1}{2}v^2(\lambda_5 - \lambda_4) \tag{23}$$

Theoretical constraints

Vacuum stability requires

$$\lambda_1 > 0, \quad \lambda_2 > 0, \quad \lambda_3 > -\sqrt{\lambda_1\lambda_2}, \quad \lambda_3 + \lambda_4 - |\lambda_5| > \sqrt{\lambda_1\lambda_2} \tag{21}$$

$$m_A^2 = \frac{m_{12}^2}{s_\beta c_\beta} - \frac{1}{2}v^2(2\lambda_5 + \frac{\lambda_6}{t_\beta} + \lambda_7 t_\beta) \tag{22}$$

$$m_{H^\pm}^2 = m_A^2 + \frac{1}{2}v^2(\lambda_5 - \lambda_4) \tag{23}$$

$m_A \in$ [10.0 GeV, 60.0 GeV], $m_h \in$ [62.5 GeV, 125.0 GeV], $m_H^\pm \in$ [89.0 GeV, 190.0 GeV], $m_{12}^2 \in$ [-1000 GeV^2, 1000 GeV^2], $\tan\beta \in$ [10, 70], $|\cos(\beta-\alpha)| \in$ [0.99, 1], $\lambda_6 \in$ [0, 0.1], $\lambda_7 \in$ [0, 0.1]

Theoretical constraints

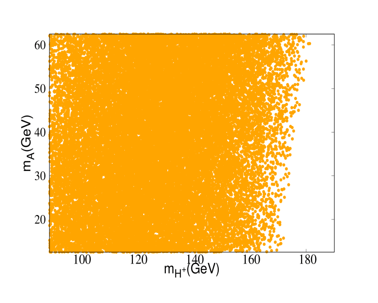

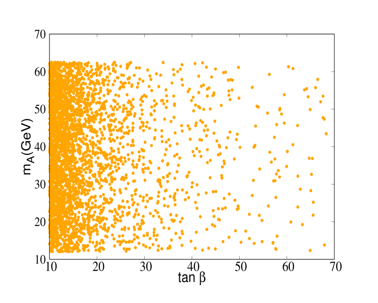

Theoretical constraints

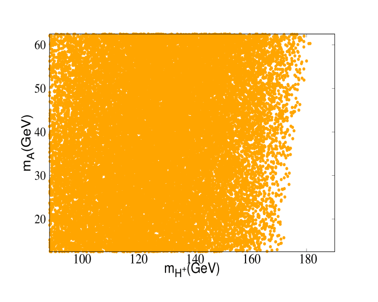

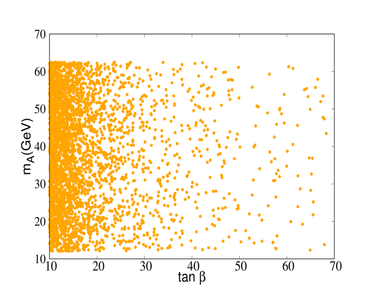

We can see that $m_H^{\pm} < 170 - 180$ GeV is allowed for low m_A . We see that although very large $tan\beta$ is allowed from perturbativity considerations, low to moderate $tan\beta$ values are much more favored compared to the high values.

Theoretical constraints

$$g_{hAA} = \frac{1}{2v}\left[(2m_A^2 - m_h^2)\frac{\cos(\alpha-3\beta)}{\sin 2\beta} + (8m_{12}^2 - \sin 2\beta(2m_A^2 + 3m_h^2))\frac{\cos(\beta+\alpha)}{\sin^2 2\beta}\right]$$
$$+v\left[\sin 2\beta \cos 2\beta(\lambda_6 - \lambda_7)\sin(\beta-\alpha) - (\lambda_6 \sin\beta \sin 3\beta + \lambda_7 \cos\beta\cos 3\beta)\cos(\beta-\alpha)\right] \quad (24)$$

The experimental upper limit on this branching ratio is rather strong in the scenario $m_A < \frac{m_h}{2}$ [9], from the search for ($pp \to h \to AA$) process in the $\mu^+\mu^-\tau^+\tau^-$ final state $\to g_{hAA}$ is extremely small. This in turn imposes a relation between m_{12}^2, $\tan\beta$ and m_A [10]. However it is required for perturbativity that $m_{12}^2 \sim \frac{m_H^2}{\tan\beta}$. In the case where 125 GeV Higgs is the lightest Higgs boson, and $m_H > 125$ GeV, it is possible to obey the perturbativity constraints as well as the upper limit on BR($h \to AA$) for low $\tan\beta < 10$ and the mass gap $m_H - m_h$ is not very large. Although this region is phenomenologically viable, the $(g_\mu - 2)$ requirements impose that m_A should also be very small, ie $m_A < 10$ GeV.

[9] CMS collaboration,JHEP 08 (2020) 139

[10] Gunion et al

Theoretical constraints

The other possibility is to consider the case when the heavier CP even Higgs is SM-like, ie $m_H = 125$ GeV. However in this case the LEP limit implies either m_A or m_h can be $< \frac{m_H}{2}$. We consider the low mass pseudoscalar, and therefore $m_h > \frac{m_H}{2}$. Here also, like the previous case the limit on BR($h \to AA$) will indicate extremely small value of the coupling g_{HAA} whose expression is given as follows:

$$g_{HAA} = \frac{1}{2v}\left[(2m_A^2 - m_H^2)\frac{\cos(\alpha - 3\beta)}{\sin 2\beta} + (8m_{12}^2 - \sin 2\beta(2m_A^2 + 3m_H^2))\frac{\cos(\beta+\alpha)}{\sin^2 2\beta}\right]$$
$$+ v\left[\sin 2\beta \cos 2\beta(\lambda_6 - \lambda_7)\cos(\beta - \alpha) + (\lambda_6 \sin\beta \sin 3\beta + \lambda_7 \cos\beta \cos 3\beta)\sin(\beta - \alpha)\right] \quad (25)$$

Theoretical constraints

The other possibility is to consider the case when the heavier CP even Higgs is SM-like, ie $m_H = 125$ GeV. However in this case the LEP limit implies either m_A or m_h can be $< \frac{m_H}{2}$. We consider the low mass pseudoscalar, and therefore $m_h > \frac{m_H}{2}$. Here also, like the previous case the limit on BR($h \to AA$) will indicate extremely small value of the coupling g_{HAA} whose expression is given as follows:

$$g_{HAA} = \frac{1}{2v}\left[(2m_A^2 - m_H^2)\frac{\cos(\alpha - 3\beta)}{\sin 2\beta} + (8m_{12}^2 - \sin 2\beta(2m_A^2 + 3m_H^2))\frac{\cos(\beta + \alpha)}{\sin^2 2\beta}\right]$$
$$+v\left[\sin 2\beta \cos 2\beta(\lambda_6 - \lambda_7)\cos(\beta - \alpha) + (\lambda_6 \sin\beta \sin 3\beta + \lambda_7 \cos\beta \cos 3\beta)\sin(\beta - \alpha)\right] \quad (25)$$

One can have a pseudoscalar mass > 10 GeV with moderate $\tan\beta$, with suitable value of m_{12}^2 and m_h, while satisfying perturbativity condition and the small BR($H \to AA$) simultaneously. This point onwards, we will explore this particular scenario, ie. for our work $m_H = 125 GeV$.

Constraints From B-Physics

In our analysis also we have taken only λ_{tt} and λ_{bb} to be non-zero where λ_{tt} and λ_{bb} are the $ht\bar{t}$ and $hb\bar{b}$ coupling strengths respectively, considering h to be the non-SM like CP-even Higgs.

[11] Phys. Rev. D69 (2004) 014002, Xiao et al and Phys. Rev. D81 (2010) 035016, Mahmoudi et al

Constraints From B-Physics

In our analysis also we have taken only λ_{tt} and λ_{bb} to be non-zero where λ_{tt} and λ_{bb} are the $ht\bar{t}$ and $hb\bar{b}$ coupling strengths respectively, considering h to be the non-SM like CP-even Higgs.

We have taken in our analysis $\lambda_{tt} \sim 0.5$ and $\lambda_{bb} \sim 2$, which allows a charged Higgs mass $m_{H^\pm} \gtrsim 150$ GeV [11].

[11] Phys. Rev. D69 (2004) 014002, Xiao et al and Phys. Rev. D81 (2010) 035016, Mahmoudi et al

Electroweak constraints

We have calculated the oblique parameter [12]

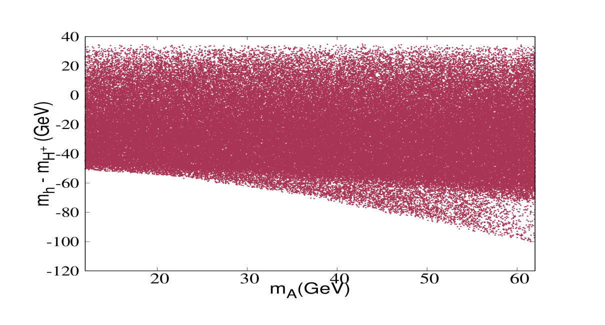

$m_h = 120$ GeV, $m_{H^\pm} = 150$ GeV.

[12] Eur. Phys. J. C78 (2018) 675, Haller et al

Constraints from collider

LEP has put a robust lower limit of 80 GeV on $m_{H^\pm}$ [13].

[13] Abbiendi et al,Eur.Phys.J.C 73 (2013) 2463
[14] ATLAS collaboration, JHEP 03 (2015) 088, CMS collaboration, JHEP 11 (2015) 018
[15] ATLAS Eur.Phys.J.C 73 (2013) 6, 2465, CMS JHEP 12 (2015) 178
[16] ATLAS-CONF-2016-088,CMS-PAS-HIG-16-031
[17] CMS-PAS-HIG-16-010

Constraints from collider

LEP has put a robust lower limit of 80 GeV on $m_{H^\pm}$ [13]. At the LHC the charged Higgs search can be categorized in two types. For $m_H^\pm < m_t$, charged Higgs can be produced from the decay of top quark($t \to bH^\pm$). This decay has been searched for in $\tau\nu$ [14] and $c\bar{s}$ [15] final state. These searches have put an upper limit on $\mathrm{BR}(t \to bH^\pm) \times (H^\pm \to \tau\nu/c\bar{s})$. The other important search mode at the LHC is $(pp \to tbH^\pm)$ in the final states $\tau\nu$ and $c\bar{s}$ [16] and $t\bar{b}$.

[13] Abbiendi et al,Eur.Phys.J.C 73 (2013) 2463

[14] ATLAS collaboration, JHEP 03 (2015) 088, CMS collaboration, JHEP 11 (2015) 018

[15] ATLAS Eur.Phys.J.C 73 (2013) 6, 2465, CMS JHEP 12 (2015) 178

[16] ATLAS-CONF-2016-088,CMS-PAS-HIG-16-031

[17] CMS-PAS-HIG-16-010

Constraints from collider

LEP has put a robust lower limit of 80 GeV on $m_{H^\pm}$ [13]. At the LHC the charged Higgs search can be categorized in two types. For $m_H^\pm < m_t$, charged Higgs can be produced from the decay of top quark($t \to bH^\pm$). This decay has been searched for in $\tau\nu$ [14] and $c\bar{s}$ [15] final state. These searches have put an upper limit on BR$(t \to bH^\pm) \times (H^\pm \to \tau\nu/c\bar{s})$. The other important search mode at the LHC is $(pp \to tbH^\pm)$ in the final states $\tau\nu$ and $c\bar{s}$ [16] and $t\bar{b}$. Collider searches for the non-standard neutral Higgs also put constraints on the parameter space of interest. Constraints from the search for low mass (pseudo)scalar produced in association with $b\bar{b}$ and decaying into $b\bar{b}$ has been taken into account. CMS has also searched for decay involving two non-standard Higgs bosons such as $h/H \to Z(\ell\ell)A(\tau\tau)$ and $h/H \to Z(\ell\ell)A(b\bar{b})$ [17]. However these limits become applicable for heavier CP-even Higgs $\gtrsim$ 200 GeV. Therefore these particular searches do not have any considerable affect on our parameter space.

[13] Abbiendi et al,Eur.Phys.J.C 73 (2013) 2463
[14] ATLAS collaboration, JHEP 03 (2015) 088, CMS collaboration, JHEP 11 (2015) 018
[15] ATLAS Eur.Phys.J.C 73 (2013) 6, 2465, CMS JHEP 12 (2015) 178
[16] ATLAS-CONF-2016-088,CMS-PAS-HIG-16-031
[17] CMS-PAS-HIG-16-010

Constraints from collider

We mention here that one should also take into account the limits coming from the direct search of the 125 GeV Higgs in various final states including $\tau\tau$,$\mu\mu$.

[18] CMS-PAS-HIG-14-040
[19] CMS collaboration,Phys.Lett.B 749 (2015) 337-362

Constraints from collider

We mention here that one should also take into account the limits coming from the direct search of the 125 GeV Higgs in various final states including $\tau\tau$,$\mu\mu$. Moreover, as the focus of our work is FCNC in the Yukawa sector, the constraints coming from flavor violating decays of 125 GeV Higgs boson also put constraints on the flavor-violating Yukawa matrix elements.

[18] CMS-PAS-HIG-14-040
[19] CMS collaboration, Phys.Lett.B 749 (2015) 337-362

Constraints from collider

We mention here that one should also take into account the limits coming from the direct search of the 125 GeV Higgs in various final states including $\tau\tau$,$\mu\mu$. Moreover, as the focus of our work is FCNC in the Yukawa sector, the constraints coming from flavor violating decays of 125 GeV Higgs boson also put constraints on the flavor-violating Yukawa matrix elements.
The 125 GeV Higgs decaying to $e\mu$ and $e\tau$ final state have been looked for by the CMS experiments [18]. CMS also puts an upper limit on the branching ratio for 125 GeV Higgs decaying to $\mu\tau$ final state [19]. Undoubtedly, these limits are crucial for our study. However, as we strictly confine ourselves to alignment limit ($\cos(\beta-\alpha)\approx 0.999$), the flavor violating decays of the 125 GeV Higgs(H in our case) will receive a suppression by a factor $\sin^2(\beta-\alpha)$.

[18] CMS-PAS-HIG-14-040
[19] CMS collaboration,Phys.Lett.B 749 (2015) 337-362

Constraints from collider

We mention here that one should also take into account the limits coming from the direct search of the 125 GeV Higgs in various final states including $\tau\tau$,$\mu\mu$. Moreover, as the focus of our work is FCNC in the Yukawa sector, the constraints coming from flavor violating decays of 125 GeV Higgs boson also put constraints on the flavor-violating Yukawa matrix elements.
The 125 GeV Higgs decaying to $e\mu$ and $e\tau$ final state have been looked for by the CMS experiments [18]. CMS also puts an upper limit on the branching ratio for 125 GeV Higgs decaying to $\mu\tau$ final state [19]. Undoubtedly, these limits are crucial for our study. However, as we strictly confine ourselves to alignment limit ($\cos(\beta-\alpha) \approx 0.999$), the flavor violating decays of the 125 GeV Higgs(H in our case) will receive a suppression by a factor $\sin^2(\beta-\alpha)$.
Therefore in this limit the constraints coming from lepton flavor violating decays of the 125 GeV Higgs are trivially satisfied.

[18] CMS-PAS-HIG-14-040

[19] CMS collaboration,Phys.Lett.B 749 (2015) 337-362

Collider

We consider probing the CP-odd scalar A in flavor violating leptonic decay mode in generalized 2HDM at the HL-LHC. Our signal process is given as

$$pp \to A \to \ell\tau_{\ell'} \tag{26}$$

where $\ell, \ell' = e, \mu$ and $\tau_{\ell'}$ denotes the leptonic decay of τ. The signal of our interest is $\ell^+\ell'^- + \not{E}_T$.

[20] JHEP03(2020)103, CMS collaboration

Collider

We consider probing the CP-odd scalar A in flavor violating leptonic decay mode in generalized 2HDM at the HL-LHC. Our signal process is given as

$$pp \to A \to \ell \tau_{\ell'} \tag{26}$$

where $\ell, \ell' = e, \mu$ and $\tau_{\ell'}$ denotes the leptonic decay of τ. The signal of our interest is $\ell^+ \ell'^- + \not{E}_T$.

The SM processes that can give rise to similar final states are $\tau\tau/ee/\mu\mu, t\bar{t}, W^{\pm}$+jets, di-boson, SM Higgs [20].

[20] JHEP03(2020)103, CMS collaboration

Collider

We consider probing the CP-odd scalar A in flavor violating leptonic decay mode in generalized 2HDM at the HL-LHC. Our signal process is given as

$$pp \to A \to \ell \tau_{\ell'} \tag{26}$$

where $\ell, \ell' = e, \mu$ and $\tau_{\ell'}$ denotes the leptonic decay of τ. The signal of our interest is $\ell^+ \ell'^- + \not{E}_T$.

The SM processes that can give rise to similar final states are $\tau\tau/ee/\mu\mu$, $t\bar{t}$, $W^{\pm}$+jets, di-boson, SM Higgs [20].

[20] JHEP03(2020)103, CMS collaboration

Collider

We mention here that since the branching ratios of the pseudoscalar decaying to flavor violating final states is very small ($\mathrm{BR}(A \to \mu\tau) \approx \mathrm{BR}(A \to \tau e) \approx 10^{-7}$), owing to the smallness of lepton flavor violating Yukawa couplings, we are compelled to choose low mass pseudoscalar which will have considerable production cross-section and therefore will be a viable candidate to search for in the collider.

	$\tan\beta$	m_A (in GeV)	m_h (in GeV)	$m_H^{\pm}$ (in GeV)	m_{12}^2 (in GeV^2)	λ_6	λ_7	$\lvert\cos(\beta-\alpha)\rvert$	$\sigma_{prod}(\sqrt{s}=14\ \mathrm{TeV})$ (in fb)
BP1	15	21	120	150	970	0.001	0.001	0.999	0.085
BP2	20	25	120	150	843	0.1	0.005	0.999	0.067
BP3	22	27	120	150	775	0.01	0.0045	0.999	0.052

Cut-Based Analysis

To generate our signal and background events, we employ the following pre-selection cuts.

$$\begin{aligned} p_T(j,b) &> 20 \text{ GeV}\,; \quad |\eta(j)| < 4.7\,; \quad |\eta(b)| < 2.5\,, \\ p_T(\ell) &> 10 \text{ GeV}\,, \quad |\eta(\ell)| < 2.5\,. \end{aligned} \tag{27}$$

The b-jets are tagged with the p_T-dependent b-tag efficiency which has an average 75% tagging efficiency of the b-jets with 50 $\text{GeV} < p_T < 200$ GeV and 1% mis-tagging efficiency for light jets.

Cut-Based Analysis

To affirm that our signal has 2 isolated leptons, we reject any third lepton with $p_T(\ell) > 10$ GeV. Moreover, since our signal is hadronically quiet, we put a jet-veto of with $p_T(j) > 20$ GeV. We also reject any b - jet with $p_T(b) > 20$ GeV. This helps us **reduce the $t\bar{t}$ semileptonic and $W^{\pm}+$ jets** background.

Cut-Based Analysis

To affirm that our signal has 2 isolated leptons, we reject any third lepton with $p_T(\ell) > 10$ GeV. Moreover, since our signal is hadronically quiet, we put a jet-veto of with $p_T(j) > 20$ GeV. We also reject any b - jet with $p_T(b) > 20$ GeV. This helps us **reduce the $t\bar{t}$ semileptonic and $W^{\pm}+$ jets** background.

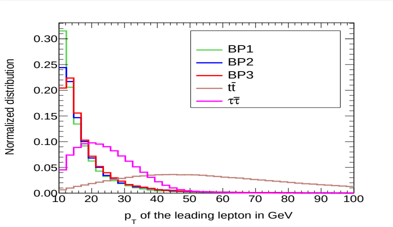

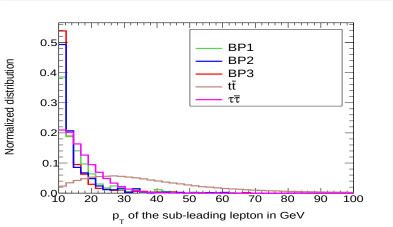

Cut-Based Analysis

The lower $\not{E}_T$ bins are populated both for signal and $\tau\tau$ background. On the other hand, top decay being a three-body decay, the $\not{E}_T$ produced in $t\bar{t}$ event peaks at a larger value.

Cut-Based Analysis

The lower $\not{E}_T$ bins are populated both for signal and $\tau\tau$ background. On the other hand, top decay being a three-body decay, the $\not{E}_T$ produced in $t\bar{t}$ event peaks at a larger value.

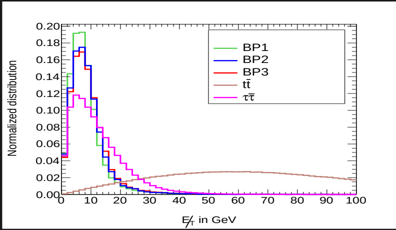

Cut-Based Analysis

The lower $\not{E}_T$ bins are populated both for signal and $\tau\tau$ background. On the other hand, top decay being a three-body decay, the $\not{E}_T$ produced in $t\bar{t}$ event peaks at a larger value.

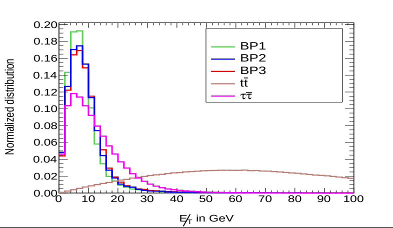

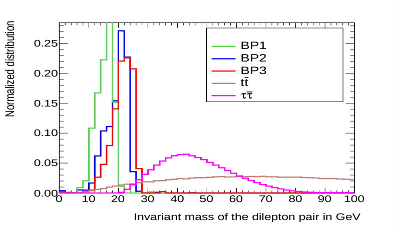

Cut-Based Analysis

The lower $\not{E}_T$ bins are populated both for signal and $\tau\tau$ background. On the other hand, top decay being a three-body decay, the $\not{E}_T$ produced in $t\bar{t}$ event peaks at a larger value.

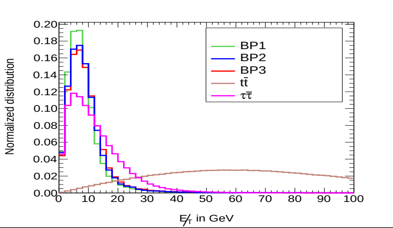

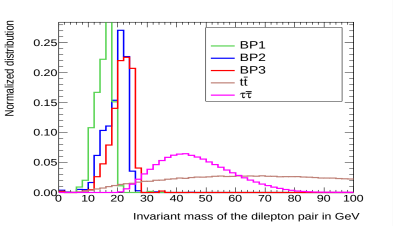

The invariant mass for $ee/\mu\mu$ peaks at a Z-boson mass and therefore a suitable cut on this variable helps us get rid of this background. In addition, $M_{\ell\ell'}$ turns out to be an important observable to **discriminate between $\tau\tau$ background and signal**.

Cut-Based Analysis

The collinear mass is defined as follows:

$$m_A = M_{collinear} = \frac{M_{vis}}{\sqrt{x_{\tau_{vis}}}},$$

with the visible momentum fraction of the τ decay products being,

$x_{\tau_{vis}} = \frac{|\vec{p}_T^{\,\tau_{vis}}|}{|\vec{p}_T^{\,\tau_{vis}}|+|\vec{p}_T^{\,\nu}|}$, where $\vec{p}_T^{\,\nu} = |\vec{\not{E}}_T|\hat{p}_T^{\,\tau_{vis}}$ and M_{vis} is the visible mass of the $\tau - \ell$ system. The variable $M_{collinear}$ essentially reconstructs the mass of the pseudoscalar. **A suitable cut should be imposed on this variable to reduce the $\tau\tau$ background**.

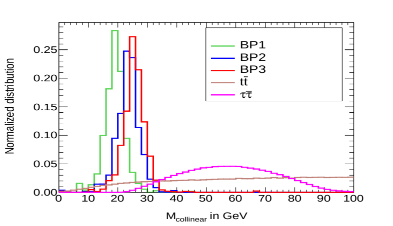

Cut-Based Analysis

The transverse mass is defined as

$$M_T(\ell) = \sqrt{2p_T(\ell)\vec{\not{E}}_T(1 - \cos\Delta\phi_{\vec{\ell}-\vec{\not{E}}_T})} \tag{28}$$

where $\Delta\phi_{\vec{\ell}-\vec{\not{E}}_T}$ denotes the azimuthal angle between the leading lepton and $\not{E}_T$. A cut on M_T variable helps us **reduce the $t\bar{t}$ background**.

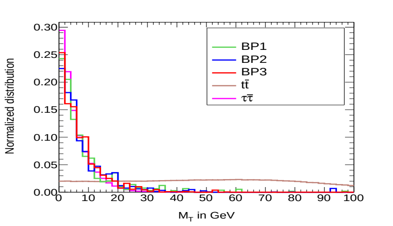

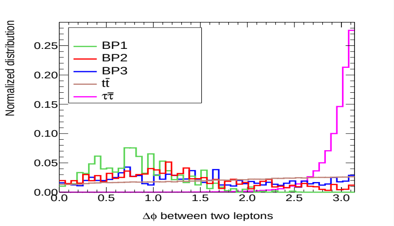

Cut-Based Analysis

SM-background	Preselection cuts	$\Delta\phi_{\ell\ell'} < 2.2$	$M_{\ell\ell'} < 15$ GeV	$E\!\!\!/_T < 15$ GeV	Mcollinear > 10 GeV	$M_T < 25$ GeV
	Effective NLO cross-section after the cut(fb)					
$\tau\tau$	8582.75	132.089	0.21	0.089	0.052	0.052
$t\bar{t}$ leptonic	22.10	11.01	0.099	0.016	0.016	0.0016
Signal						
BP1	0.0689	0.0686	0.0276	0.0266	0.0262	0.0258
BP2	0.0637	0.0542	0.0081	0.0076	0.0073	0.0073
BP3	0.0513	0.0381	0.0028	0.0026	0.0025	0.0025

Benchmark points	Significance reach at 3 ab^{-1} luminosity
BP1	5.7 σ
BP2	1.7 σ
BP3	0.6 σ

[21] Eur. Phys. J. C71 (2011) 1554, Cowan et al

Cut-Based Analysis

	Effective NLO cross-section after the cut(fb)					
SM-background	Preselection cuts	$\Delta\phi_{\ell\ell'} < 2.2$	$M_{\ell\ell'} < 15$ GeV	$\not{E}_T < 15$ GeV	Mcollinear > 10 GeV	$M_T < 25$ GeV
$\tau\tau$	8582.75	132.089	0.21	0.089	0.052	0.052
$t\bar{t}$ leptonic	22.10	11.01	0.099	0.016	0.016	0.0016
Signal						
BP1	0.0689	0.0686	0.0276	0.0266	0.0262	0.0258
BP2	0.0637	0.0542	0.0081	0.0076	0.0073	0.0073
BP3	0.0513	0.0381	0.0028	0.0026	0.0025	0.0025

Benchmark points	Significance reach at 3 ab^{-1} luminosity
BP1	5.7 σ
BP2	1.7 σ
BP3	0.6 σ

The significance [21] is calculated using the following formula.

$$\mathcal{S} = \sqrt{2[(S+B)ln(1+\frac{S}{B}) - S]}$$

[21] Eur. Phys. J. C71 (2011) 1554, Cowan et al

ANN

Variable	Definition
$p_T^{\ell_1}$	Transverse momentum of the leading lepton
$p_T^{\ell_2}$	Transverse momentum of the sub-leading lepton
E_T^{miss}	Missing transverse energy
$M_{\ell\ell'}$	Invariant mass of the di-lepton pair
$\Delta\phi_{\ell\ell'}$	Azimuthal angle difference between the di-lepton pair
$\Delta R_{\ell\ell'}$	ΔR separation between the di-lepton pair
M_{vis}	Visible mass of the di-lepton system
x_{vis}	Visible momentum fraction of the τ decay products
$M_{collinear}$	Collinear mass
M_T	Transverse mass
$\Delta\phi_{\ell_1 \not{E}_T}$	Azimuthal angle difference between the leading lepton and $\not{E}_T$
$\Delta\phi_{\ell_2 \not{E}_T}$	Azimuthal angle difference between the sub-leading lepton and $\not{E}_T$

ANN

For ANN analysis we have chosen a network with four hidden layers with activation curve relu at all of them. The batch-size is taken to be 1000 and the number of epochs is 100 in our case for each batch. We have used 80% of the dataset for training and 20% for validation.
In order to obtain a better performance from the network we have applied two basic cuts, namely $M_{\ell\ell'} < 30$ GeV and $M_{collinear} < 40$ GeV on signal and background events over and above the lepton selection and jet-veto.

ANN

For ANN analysis we have chosen a network with four hidden layers with activation curve relu at all of them. The batch-size is taken to be 1000 and the number of epochs is 100 in our case for each batch. We have used 80% of the dataset for training and 20% for validation.
In order to obtain a better performance from the network we have applied two basic cuts, namely $M_{\ell\ell'} < 30$ GeV and $M_{collinear} < 40$ GeV on signal and background events over and above the lepton selection and jet-veto.
Therefore the network will be trained better to separate signal from background specifically in the signal region, this results in a better accuracy in the output. The accuracy we get is 99%(BP1), 98%(BP2) and 96%(BP3) which indicates very good discriminating power between signal and background.

ANN

For ANN analysis we have chosen a network with four hidden layers with activation curve relu at all of them. The batch-size is taken to be 1000 and the number of epochs is 100 in our case for each batch. We have used 80% of the dataset for training and 20% for validation.
In order to obtain a better performance from the network we have applied two basic cuts, namely $M_{\ell\ell'} < 30$ GeV and $M_{collinear} < 40$ GeV on signal and background events over and above the lepton selection and jet-veto.
Therefore the network will be trained better to separate signal from background specifically in the signal region, this results in a better accuracy in the output. The accuracy we get is 99%(BP1), 98%(BP2) and 96%(BP3) which indicates very good discriminating power between signal and background.
The area under curve is 0.999(BP1), 0.998(BP2) and 0.994(BP3).

ANN

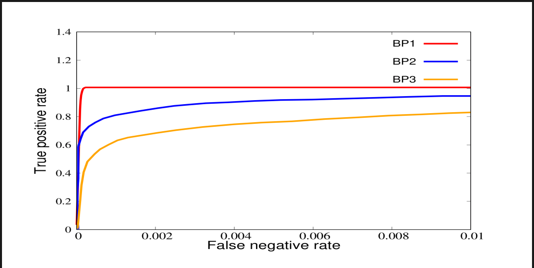
BP1
BP2
BP3
True positive rate
False negative rate
0
0.2
0.4
0.6
0.8
1
1.2
1.4
0
0.002
0.004
0.006
0.008
0.01

ANN

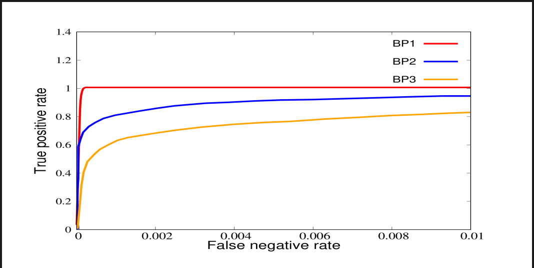

BP	$\mathcal{S}$ (cuts+ANN)
BP1	9.2 σ
BP2	5.3 σ
BP3	3.2 σ

Conclusion

- We show that the long-standing problem of muon anomaly and LFV constraints can be solved simultaneously over considerable range of parameter space in this model with flavor changing couplings fixed at $y_{\mu e} = 10^{-7}, y_{\tau e} = 5 \times 10^{-5}$ and $y_{\mu\tau} = 5 \times 10^{-5}$ and the non-standard CP-even and charged Higgs masses are fixed at 120 GeV and 150 GeV respectively.

Conclusion

- We show that the long-standing problem of muon anomaly and LFV constraints can be solved simultaneously over considerable range of parameter space in this model with flavor changing couplings fixed at $y_{\mu e} = 10^{-7}, y_{\tau e} = 5 \times 10^{-5}$ and $y_{\mu\tau} = 5 \times 10^{-5}$ and the non-standard CP-even and charged Higgs masses are fixed at 120 GeV and 150 GeV respectively.
- After finding out the region allowed by all constraints, we look for flavor violating decay of CP-odd scalar (A) in the $\ell\tau \to \ell^+\ell'^- + \not{E}_T$ final state, where τ decays leptonically and $\ell, \ell' = e, \mu$.

Conclusion

- We show that the long-standing problem of muon anomaly and LFV constraints can be solved simultaneously over considerable range of parameter space in this model with flavor changing couplings fixed at $y_{\mu e} = 10^{-7}, y_{\tau e} = 5 \times 10^{-5}$ and $y_{\mu\tau} = 5 \times 10^{-5}$ and the non-standard CP-even and charged Higgs masses are fixed at 120 GeV and 150 GeV respectively.
- After finding out the region allowed by all constraints, we look for flavor violating decay of CP-odd scalar (A) in the $\ell\tau \to \ell^+\ell'^- + \not{E}_T$ final state, where τ decays leptonically and $\ell, \ell' = e, \mu$.
- Performing a rectangular cut-based analysis for 14 TeV LHC with $3ab^{-1}$ luminosity, we show that the significance drops from $\sim 6\sigma$ to $\sim 1\sigma$ as the mass of the scalar increases from 21 GeV to 27 GeV which definitely improves in ANN.

Conclusion

- We show that the long-standing problem of muon anomaly and LFV constraints can be solved simultaneously over considerable range of parameter space in this model with flavor changing couplings fixed at $y_{\mu e} = 10^{-7}, y_{\tau e} = 5 \times 10^{-5}$ and $y_{\mu\tau} = 5 \times 10^{-5}$ and the non-standard CP-even and charged Higgs masses are fixed at 120 GeV and 150 GeV respectively.
- After finding out the region allowed by all constraints, we look for flavor violating decay of CP-odd scalar (A) in the $\ell\tau \to \ell^+\ell'^- + \not{E}_T$ final state, where τ decays leptonically and $\ell, \ell' = e, \mu$.
- Performing a rectangular cut-based analysis for 14 TeV LHC with $3ab^{-1}$ luminosity, we show that the significance drops from $\sim 6\sigma$ to $\sim 1\sigma$ as the mass of the scalar increases from 21 GeV to 27 GeV which definitely improves in ANN.

B-physics

The most stringent constraint comes from the $B \to X_s\gamma$ decay. The impact of these constraints in terms of specific types of 2HDM as well as in generalised 2HDM have been studied in great detail in earlier works [22]. In conventional type I and type II 2HDM, the dominant additional contribution to the loop induced decay $B \to X_s\gamma$ comes from the charged Higgs boson-top quark penguin diagrams and its contribution depends on $m_{H^\pm}$. In type II 2HDM, this extra contribution interferes constructively with its SM counterpart and therefore the lower bound on the charged Higgs boson becomes rather high ($m_H^\pm \gtrsim 600$ GeV). In type I, the charged Higgs penguin diagram's contribution interferes destructively with its SM counterpart and gives negligible result at large $\tan\beta$. The type X model has same structure as type I, as far as the interactions of Higgs with the quark sector is concerned. Therefore Type X models also do not receive any strong lower bound on $m_{H^\pm}$. As we can think of our model as a perturbation from the type X scenario, in the absence of the extra terms in the Yukawa Lagrangian, there is no strict lower bound on the charged Higgs mass. However, even in the presence of non-zero FCNC Yukawa matrix elements, it is possible to have low enough charged Higgs mass with suitable choice of λ_{tt} and λ_{bb} couplings. We have taken in our analysis $\lambda_{tt} \sim 0.5$ and $\lambda_{bb} \sim 2$, which allows a charged Higgs mass $m_{H^\pm} \gtrsim 150$ GeV.

[22] Crivellin et al, Phys.Rev.D 87 (2013) 9, 094031

B-physics

Another decay process which can constrain our model parameters space is $B^{\pm} \to \tau^{\pm}\nu_{\tau}$ where charged Higgs enters at the tree level itself. The observed branching ratio for the process $B_u^{\pm} \to \tau^{\pm}\nu_{\tau} = (1.06 \pm 0.19) \times 10^{-4}$ [23]. The decay $B_c^{\pm} \to \tau^{\pm}\nu_{\tau}$, although has not been observed, but puts an upper limit ($< 30\%$) on the branching ratio for this decay. However, we have assumed only λ_{tt} and λ_{bb} are non-zero in the quark sector, we find out that these limits essentially reduces to a limit on λ_{bb} and $\tan\beta$. In [24], it has been shown that $\lambda_{bb} \sim 2$ is favored for large or moderate $\tan\beta$.

The constraint from ΔM_B puts an an upper limit on λ_{tt} as a function of the charged Higgs mass [25]. $m_{H^{\pm}} \gtrsim 150$ GeV is allowed for $\lambda_{tt} \lesssim 0.5$.

The upper limit on the BR($B_s \to \mu^+\mu^-$) is $2.4^{+0.9}_{-0.7} \times 10^{-9}$ [26]. This particular branching fraction constrains the low $\tan\beta (< 2)$ region for low $m_H^{\pm} (\sim 100$ GeV) [27]. For higher charged Higgs mass this limit is further relaxed.

[23] Alonso et al, Phys. Rev. Lett. 118 (2017) 081802

[24] Arhrib et al, Arxiv:1710.05898

[25] Mahmoudi et al, Phys.Rev.D 81 (2010) 035016

[26] Patrignani et al, Chin.Phys.C 40 (2016) 10, 100001

[27] Arbey et al, Eur.Phys.J.C 78 (2018) 3, 182

The collinear mass is defined as follows:

$$m_A = M_{collinear} = \frac{M_{vis}}{\sqrt{x_{\tau_{vis}}}},$$

with the visible momentum fraction of the τ decay products being,
$x_{\tau_{vis}} = \frac{|\vec{p}_T^{\,\tau_{vis}}|}{|\vec{p}_T^{\,\tau_{vis}}|+|\vec{p}_T^{\,\nu}|}$, where $\vec{p}_T^{\,\nu} = |\vec{\not{E}}_T|\hat{p}_T^{\,\tau_{vis}}$ and M_{vis} is the visible mass of the $\tau - \ell$ system. The variable $M_{collinear}$ essentially reconstructs the mass of the pseudoscalar.

$$M_T(\ell) = \sqrt{2p_T(\ell)\vec{\not{E}}_T(1 - \cos\Delta\phi_{\vec{\ell}-\vec{\not{E}}_T})} \tag{29}$$

where $\Delta\phi_{\vec{\ell}-\vec{\not{E}}_T}$ denotes the azimuthal angle between the leading lepton and $\not{E}_T$.